Z Production Cross Sections and Lepton Pair Forward-Backward Asymmetries

The ALEPH Collaboration[1]

Abstract

Precise values of the Z resonance cross sections and lepton pair forward-backward asymmetries are measured from a sample of 1.3 million Z decays into hadrons and charged leptons taken with the ALEPH detector at LEP. A silicon-tungsten luminosity calorimeter was installed in ALEPH in 1992, permitting the determination of the absolute luminosity to a systematic precision of 0.15% (experimental) and 0.25% (theoretical). This is combined with a better understanding of the hadronic event selection and an improved tau pair selection. Including the ALEPH results of the past three years one obtains $\sigma_h^0 = (41.60 \pm 0.16)$ nb, and $R_l = 20.69 \pm 0.09$. The corresponding number of light neutrino species is $N_\nu = 2.983 \pm 0.034$. The lepton pair forward-backward asymmetry is used to derive the ratio of vector to axial-vector couplings of leptons: $g_V^2(M_Z^2)/g_A^2(M_Z^2) = 0.0058 \pm 0.0011$. An application of these results to constrain one model with extra Z bosons is presented.

---

[1]See the following pages for the list of authors.

The ALEPH Collaboration

D. Buskulic, D. Casper, I. De Bonis, D. Decamp, P. Ghez, C. Goy, J.-P. Lees, M.-N. Minard, P. Odier, B. Pietrzyk

Laboratoire de Physique des Particules (LAPP), IN²P³-CNRS, 74019 Annecy-le-Vieux Cedex, France

F. Ariztizabal, P. Comas, J.M. Crespo, I. Efthymiopoulos, E. Fernandez, M. Fernandez-Bosman, V. Gaitan, Ll. Garrido,[29] M. Martinez, T. Mattison,[30] S. Orteu, A. Pacheco, C. Padilla, A. Pascual

Institut de Fisica d'Altes Energies, Universitat Autonoma de Barcelona, 08193 Bellaterra (Barcelona), Spain[7]

D. Creanza, M. de Palma, A. Farilla, G. Iaselli, G. Maggi, N. Marinelli, S. Natali, S. Nuzzo, A. Ranieri, G. Raso, F. Romano, F. Ruggieri, G. Selvaggi, L. Silvestris, P. Tempesta, G. Zito

Dipartimento di Fisica, INFN Sezione di Bari, 70126 Bari, Italy

Y. Chai, D. Huang, X. Huang, J. Lin, T. Wang, Y. Xie, D. Xu, R. Xu, J. Zhang, L. Zhang, W. Zhao

Institute of High-Energy Physics, Academia Sinica, Beijing, The People's Republic of China[8]

G. Bonvicini, J. Boudreau,[25] H. Drevermann, R.W. Forty, G. Ganis, C. Gay,[3] M. Girone, R. Hagelberg, J. Harvey, J. Hilgart,[27] R. Jacobsen, B. Jost, J. Knobloch, I. Lehraus, M. Maggi, C. Markou, P. Mato, H. Meinhard, A. Minten, R. Miquel, K. Moffeit, P. Palazzi, J.R. Pater, J.A. Perlas, P. Perrodo, J.-F. Pusztaszeri, F. Ranjard, L. Rolandi, J. Rothberg,[2] T. Ruan, M. Saich, D. Schlatter, M. Schmelling, F. Sefkow,[6] W. Tejessy, I.R. Tomalin, R. Veenhof, H. Wachsmuth, S. Wasserbaech,[2] W. Wiedenmann, T. Wildish, W. Witzeling, J. Wotschack

European Laboratory for Particle Physics (CERN), 1211 Geneva 23, Switzerland

Z. Ajaltouni, M. Bardadin-Otwinowska, A. Barres, C. Boyer, A. Falvard, P. Gay, C. Guicheney, P. Henrard, J. Jousset, B. Michel, J-C. Montret, D. Pallin, P. Perret, F. Podlyski, J. Proriol, F. Saadi

Laboratoire de Physique Corpusculaire, Université Blaise Pascal, IN²P³-CNRS, Clermont-Ferrand, 63177 Aubière, France

T. Fearnley, J.B. Hansen, J.D. Hansen, J.R. Hansen, P.H. Hansen, S.D. Johnson, R. Møllerud, B.S. Nilsson[1]

Niels Bohr Institute, 2100 Copenhagen, Denmark[9]

A. Kyriakis, E. Simopoulou, I. Siotis, A. Vayaki, K. Zachariadou

Nuclear Research Center Demokritos (NRCD), Athens, Greece

J. Badier, A. Blondel, G. Bonneaud, J.C. Brient, P. Bourdon, G. Fouque, L. Passalacqua, A. Rougé, M. Rumpf, R. Tanaka, M. Verderi, H. Videau

Laboratoire de Physique Nucléaire et des Hautes Energies, Ecole Polytechnique, IN²P³-CNRS, 91128 Palaiseau Cedex, France

D.J. Candlin, M.I. Parsons, E. Veitch

Department of Physics, University of Edinburgh, Edinburgh EH9 3JZ, United Kingdom[10]

E. Focardi, L. Moneta, G. Parrini

Dipartimento di Fisica, Università di Firenze, INFN Sezione di Firenze, 50125 Firenze, Italy

M. Corden, M. Delfino,[12] C. Georgiopoulos, D.E. Jaffe, D. Levinthal[15]

Supercomputer Computations Research Institute, Florida State University, Tallahassee, FL 32306-4052, USA [13,14]

A. Antonelli, G. Bencivenni, G. Bologna,[4] F. Bossi, P. Campana, G. Capon, F. Cerutti, V. Chiarella, G. Felici, P. Laurelli, G. Mannocchi,[5] F. Murtas, G.P. Murtas, M. Pepe-Altarelli, S. Salomone

Laboratori Nazionali dell'INFN (LNF-INFN), 00044 Frascati, Italy

P. Colrain, I. ten Have, I.G. Knowles, J.G. Lynch, W. Maitland, W.T. Morton, C. Raine, P. Reeves, J.M. Scarr, K. Smith, M.G. Smith, A.S. Thompson, S. Thorn, R.M. Turnbull

Department of Physics and Astronomy, University of Glasgow, Glasgow G12 8QQ, United Kingdom[10]

U. Becker, O. Braun, C. Geweniger, P. Hanke, V. Hepp, E.E. Kluge, A. Putzer,[1] B. Rensch, M. Schmidt H. Stenzel, K. Tittel, M. Wunsch

Institut für Hochenergiephysik, Universität Heidelberg, 69120 Heidelberg, Fed. Rep. of Germany[16]

R. Beuselinck, D.M. Binnie, W. Cameron, M. Cattaneo, D.J. Colling, P.J. Dornan, J.F. Hassard, N. Konstantinidis, A. Moutoussi, J. Nash, D.G. Payne, G. San Martin, J.K. Sedgbeer, A.G. Wright

Department of Physics, Imperial College, London SW7 2BZ, United Kingdom[10]

P. Girtler, D. Kuhn, G. Rudolph, R. Vogl

Institut für Experimentalphysik, Universität Innsbruck, 6020 Innsbruck, Austria[18]

C.K. Bowdery, T.J. Brodbeck, A.J. Finch, F. Foster, G. Hughes, D. Jackson, N.R. Keemer, M. Nuttall, A. Patel, T. Sloan, S.W. Snow, E.P. Whelan

Department of Physics, University of Lancaster, Lancaster LA1 4YB, United Kingdom[10]

A. Galla, A.M. Greene, K. Kleinknecht, J. Raab, B. Renk, H.-G. Sander, H. Schmidt, S.M. Walther, R. Wanke, B. Wolf

Institut für Physik, Universität Mainz, 55099 Mainz, Fed. Rep. of Germany[16]

A.M. Bencheikh, C. Benchouk, A. Bonissent, D. Calvet, J. Carr, P. Coyle, C. Diaconu, F. Etienne, D. Nicod, P. Payre, L. Roos, D. Rousseau, P. Schwemling, M. Talby

Centre de Physique des Particules, Faculté des Sciences de Luminy, IN^2P^3-CNRS, 13288 Marseille, France

3

S. Adlung, R. Assmann, C. Bauer, W. Blum, D. Brown, P. Cattaneo,[23] B. Dehning, H. Dietl, F. Dydak,[21] M. Frank, A.W. Halley, K. Jakobs, J. Lauber, G. Lütjens, G. Lutz, W. Männer, H.-G. Moser, R. Richter, J. Schröder, A.S. Schwarz, R. Settles, H. Seywerd, U. Stierlin, U. Stiegler, R. St. Denis, G. Wolf

Max-Planck-Institut für Physik, Werner-Heisenberg-Institut, 80805 München, Fed. Rep. of Germany[16]

R. Alemany, J. Boucrot,[1] O. Callot, A. Cordier, M. Davier, L. Duflot, J.-F. Grivaz, Ph. Heusse, P. Janot, D.W. Kim,[19] F. Le Diberder, J. Lefrançois, A.-M. Lutz, G. Musolino, M.-H. Schune, J.-J. Veillet, I. Videau

Laboratoire de l'Accélérateur Linéaire, Université de Paris-Sud, IN^2P^3-CNRS, 91405 Orsay Cedex, France

D. Abbaneo, G. Bagliesi, G. Batignani, U. Bottigli, C. Bozzi, G. Calderini, M. Carpinelli, M.A. Ciocci, V. Ciulli, R. Dell'Orso, I. Ferrante, F. Fidecaro, L. Foà,[1] F. Forti, A. Giassi, M.A. Giorgi, A. Gregorio, F. Ligabue, A. Lusiani, P.S. Marrocchesi, E.B. Martin, A. Messineo, F. Palla, G. Rizzo, G. Sanguinetti, P. Spagnolo, J. Steinberger, R. Tenchini,[1] G. Tonelli,[28] G. Triggiani, A. Valassi, C. Vannini, A. Venturi, P.G. Verdini, J. Walsh

Dipartimento di Fisica dell'Università, INFN Sezione di Pisa, e Scuola Normale Superiore, 56010 Pisa, Italy

A.P. Betteridge, Y. Gao, M.G. Green, D.L. Johnson, P.V. March, T. Medcalf, Ll.M. Mir, I.S. Quazi, J.A. Strong

Department of Physics, Royal Holloway & Bedford New College, University of London, Surrey TW20 OEX, United Kingdom[10]

V. Bertin, D.R. Botterill, R.W. Clifft, T.R. Edgecock, S. Haywood, M. Edwards, P.R. Norton, J.C. Thompson

Particle Physics Dept., Rutherford Appleton Laboratory, Chilton, Didcot, Oxon OX11 OQX, United Kingdom[10]

B. Bloch-Devaux, P. Colas, H. Duarte, S. Emery, W. Kozanecki, E. Lançon, M.C. Lemaire, E. Locci, B. Marx, P. Perez, J. Rander, J.-F. Renardy, A. Rosowsky, A. Roussarie, J.-P. Schuller, J. Schwindling, D. Si Mohand, B. Vallage

Service de Physique des Particules, DAPNIA, CE-Saclay, 91191 Gif-sur-Yvette Cedex, France[17]

R.P. Johnson, A.M. Litke, G. Taylor, J. Wear

Institute for Particle Physics, University of California at Santa Cruz, Santa Cruz, CA 95064, USA[22]

W. Babbage, E. Beddall C.N. Booth, S. Cartwright, F. Combley, I. Dawson, C. Rankin, L.F. Thompson

Department of Physics, University of Sheffield, Sheffield S3 7RH, United Kingdom[10]

A. Böhrer, S. Brandt, G. Cowan,[1] E. Feigl, C. Grupen, G. Lutters, J. Minguet-Rodriguez, F. Rivera,[26] P. Saraiva, U. Schäfer, L. Smolik

Fachbereich Physik, Universität Siegen, 57068 Siegen, Fed. Rep. of Germany[16]

4

L. Bosisio, R. Della Marina, G. Giannini, B. Gobbo, L. Pitis, F. Ragusa[20]

Dipartimento di Fisica, Università di Trieste e INFN Sezione di Trieste, 34127 Trieste, Italy

L. Bellantoni, W. Chen, J.S. Conway,[24] Z. Feng, D.P.S. Ferguson, Y.S. Gao, J. Grahl, J.L. Harton, O.J. Hayes, H. Hu, J.M. Nachtman, Y.B. Pan, Y. Saadi, M. Schmitt, I. Scott, V. Sharma, J.D. Turk, A.M. Walsh, F.V. Weber, Sau Lan Wu, X. Wu, M. Zheng, J.M. Yamartino, G. Zobernig

Department of Physics, University of Wisconsin, Madison, WI 53706, USA[11]

1 Introduction

The precision of the absolute cross section measurements in ALEPH has been improved with the installation in September 1992 of a silicon-tungsten luminosity monitor (SiCAL). Additional improvements over previous ALEPH publications [1, 2] come from a re-evaluation of the systematic error in the hadron selection and an improved tau-pair selection. Only the differences between the present analysis and that previously published are described in detail.

The ALEPH detector has been described elsewhere [3]. The SiCAL upgrade introduced two luminosity setups for the measurements in 1992 for which the data were analyzed separately:

1. **LCAL period**: luminosity measurements up to the September 1992 LEP technical stop were performed with the lead-proportional wire chamber calorimeter (LCAL) alone. The horizontal separation between the two halves of both LCAL calorimeters was increased by 5 mm to reduce shadowing effects from SiCAL when it is in place.

2. **SiCAL period**: luminosity measurements after the September 1992 step were performed with the SiCAL. Since a detailed description of the SiCAL construction and performance is in preparation [4], only aspects relevant to the cross section measurements are included here.

The analysis presented here is based upon a sample of 780 000 charged fermion pairs collected by ALEPH at LEP in 1992, representing an integrated luminosity of 13.7 pb^{-1} in the LCAL period ($\sqrt{s} = (91.276 \pm 0.018)$ GeV) and 8.7 pb^{-1} in the SiCAL period ($\sqrt{s} = (91.270 \pm 0.018)$ GeV). The LEP energies are given by the LEP energy group [5]. The fit results presented here are based upon 1 300 000 visible Z decays to fermion pairs accumulated by ALEPH over the past four years of data collection.

2 Luminosity Determination

2.1 LCAL Luminosity Measurement

The luminosity determination with the LCAL, covering the polar angular region from 46 to 122 mrad, has been described in detail elsewhere [6]. The evaluation of the systematic error for 1992 proceeded in the same way as in the previous years. To check the accuracy of the understanding of the acceptance, the results using two different fiducial-side selections [6] were compared. The difference using all LCAL data from 1989 to 1992 is compatible with a systematic error of 0.21%, whose determination with this method has fluctuated statistically from year to year. The total LCAL experimental systematic errors for this and the previous years become: 0.49% (1989–1990), 0.38% (1991) and 0.37% (1992 LCAL period) and are used in the electroweak fits.

2.2 SiCAL Luminosity

The SiCAL is a silicon-tungsten sampling electromagnetic calorimeter, 23 radiation lengths (X_0) in depth. It consists of two homogeneous cylindrical detectors surrounding the beam pipe at roughly ± 250 cm from the interaction point. The calorimeters cover the polar angular range from 24 to 58 mrad. Twelve layers of tungsten alternate with layers of silicon pad detectors. Each layer is segmented into 32 sectors in azimuth, each with 16 radial pad rows 5.225 mm wide. A total of 12288 pads are readout individually, allowing a full reconstruction of the transverse and longitudinal shower development. The internal alignment of the silicon detector elements and the measurement of the separation between half modules with a light-emitting diode optical system ensure a mechanical precision of the radial fiducial boundary of 18μm.

The analysis of the 1992 SiCAL luminosity is largely based upon the previous LCAL analysis [6], simplified by the homogeneity of the new detector. Bhabha scatterings are identified by requiring at least one reconstructed cluster in each endcap, side A and side B, with an energy $\geq$ 20 GeV. The sum of their energies must be $\geq$ 55 GeV. The acoplanarity of these clusters is restricted to $150° \leq \Delta\phi \leq 210°$ in order to remove background from accidental coincidences of off-momentum beam particles. Radial cuts define the Bhabha acceptance. Energy sharing between pads at the fiducial boundary, summed over two layers in depth at $6X_0$ and $8X_0$, is used to determine the acceptance near the boundary. A "tight" fiducial selection on one side and a "loose" fiducial selection on the opposite side, alternated event by event, reduce the sensitivity of the selection to beam offsets. The tight side is sufficiently constrained to ensure full containment of showers from Bhabha events (radial pad rows 4 to 12, inclusively), whereas the loose side permits clusters to lie within pad rows 2 to 15, inclusively.

There is very good agreement between the data and the Monte Carlo simulation used to integrate the accepted low angle Bhabha cross section. Figure 1 shows the radial distribution for tight-side selected clusters, and Figure 2 shows the azimuthal distributions for events accepted with either side's tight radial selections. The periodic variation in ϕ is due to the offset of the beam with respect to the detector axis; it is well reproduced by the simulation.

The background to the luminosity selection comes almost entirely from two sources: 1) accidental coincidences of off-momentum beam particles, and 2) t-channel production of two or more hard photons, indistinguishable from a Bhabha scattering in this purely calorimetric monitor. The off-momentum background is evaluated using the SiCAL single-arm triggers and is found to be $8.5 \cdot 10^{-4}$ of the Bhabha rate, and is subtracted from the data. The t-channel hard photon background is calculated and used to correct the accepted Bhabha cross section; it corresponds to a 0.015% contamination of the selection. Other physics processes produce a background below 0.010%.

Two cross-checks were used to verify the understanding of the Bhabha acceptance. First, the radius of the tight fiducial boundary was decreased by one padwidth; the ratio of accepted events to the Bhabha selection gives 1.237 ± 0.001 for data in good agreement with 1.238 ± 0.001 for the Monte Carlo simulation. Second, two independent azimuthal selections, sensitive to systematics from background subtraction or half-module separations, were compared: "horizontal" events were required to be in the horizontal plane $\pm 33.75°$ and "vertical" events were required to be in the vertical plane $\pm 33.75°$. The ratio of horizontally to vertically selected Bhabhas gives 1.003 ± 0.003 for data, in agreement with 1.006 ± 0.003 found for the Monte Carlo.

The experimental systematic errors are summarized in Table 1. The mechanical precision combined with the uncertainty on the z-distance between the calorimeters gives an ultimate luminosity precision of 0.068%. Although more than two million Bhabha events were processed through the ALEPH simulation and reconstruction package, the 1992 estimated experimental precision is limited by the Monte Carlo statistics: $0.15\% = 0.09\%(exp.) \oplus 0.12\%(mc\ stat.)$. This is still reasonable given the statistical precision of the Z sample. The additional sources of experimental systematics come primarily from effects such as pad-to-pad energy precision and simulation of showers within the detector.

2.3 LCAL-SiCAL Relative Luminosity Measurements

Two comparisons of the LCAL and SiCAL luminosity measurements were performed to cross-check the LCAL measurements. First, indirectly, a fit to the hadronic cross section in the LCAL periods (1989 to September 1992) is compared to the hadronic cross section in the SiCAL period, the former corrected for the difference in $\sqrt{s}$. The ratio of the hadron cross section measured with SiCAL to the LCAL (energy corrected) cross section is 0.9981 ± 0.0046, where the statistical and systematic errors are combined, excluding the luminosity theoretical error discussed below.

7

ALEPH
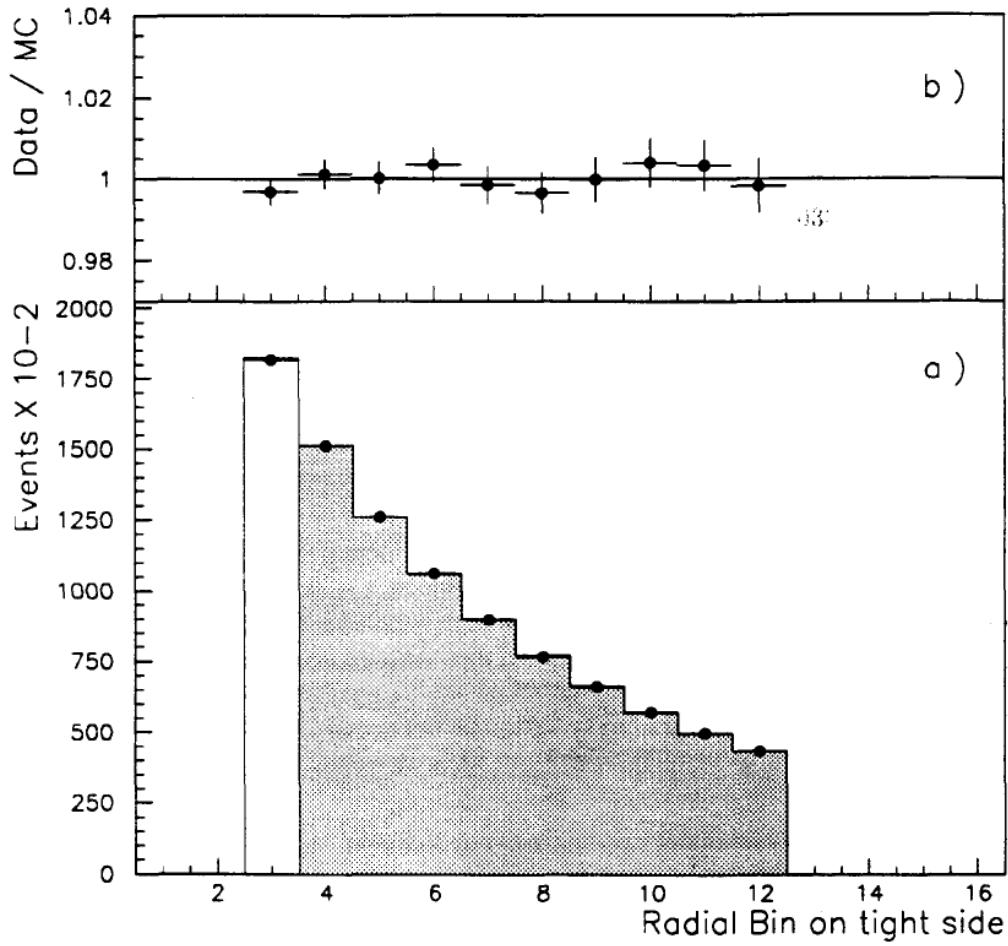
Figure 1: a) Radial distribution for the tight-side selection (final selection shown as shaded zone). Data are plotted as points; Monte Carlo shown as a histogram.
b) Ratio of data to Monte Carlo.
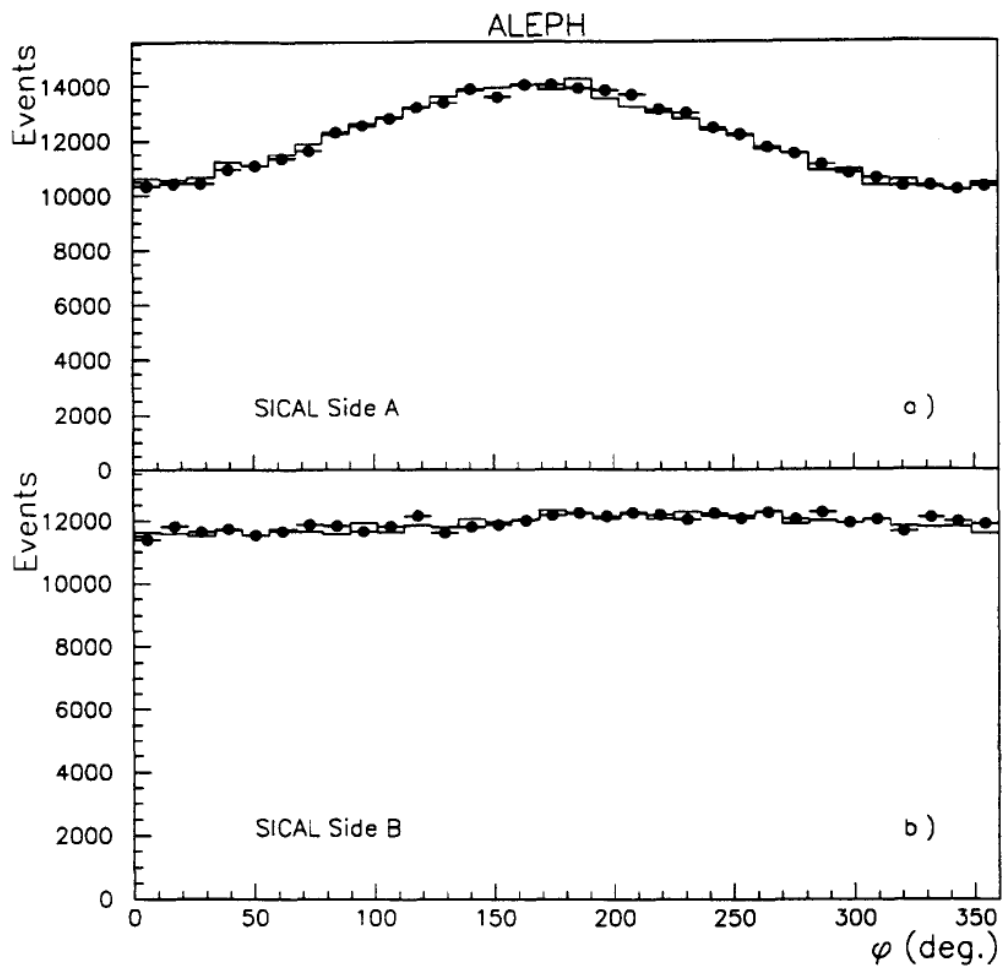
Figure 2:   a) ϕ distribution for side A tight selection.
b) ϕ distribution for side B tight selection, for accepted Bhabha events. The data are plotted as points and the Monte Carlo is shown as a histogram. The ϕ variation is due to different offsets of the beam with respect to the axes of the side A and side B detectors.

9

Background estimation:	
– Off-momentum beam particles	0.018%
– Physics sources	0.010%
Trigger efficiency	0.010%
Radial fiducial cuts:	
– mechanical precision and z position	0.068%
– beam-module relative tilt and alignments	0.035%
– energy sharing cuts	0.044%
– shower parametrization and simulation	0.023%
Energy cuts	0.015%
Acoplanarity cut	0.005%
Simulation statistics	0.120%
TOTAL experimental uncertainty	0.153%

Table 1: Summary of SiCAL luminosity systematic errors.

A second, direct test was made comparing the LCAL measured luminosity during the SiCAL period. In contrast to previous years, the SiCAL shadow below 59 mrad on the LCAL detector could slightly disturb the latter's precision. The ratio between the LCAL and SiCAL integrated luminosities in the SiCAL period is 0.9988 ± 0.0039 (stat) ± 0.0039 (syst), where the statistical error includes both data and Monte Carlo simulation statistics and the systematic error excludes the theoretical uncertainty. The shadowing effect is included and is estimated to contribute an uncertainty of $\leq 0.1\%$.

Combining the two tests, and interpreting the ratio of hadron cross sections as a luminosity ratio, gives an LCAL to SiCAL luminosity measurement ratio of 0.9984 ± 0.0027(stat) ± 0.0034(syst).

2.4 Luminosity Theoretical Error

The Bhabha reference cross sections for LCAL and SiCAL acceptances during both periods have been calculated using the Monte Carlo program BHLUMI [7]. BHLUMI is a multi-photon $\mathcal{O}(\alpha)$ event generator with exclusive exponentiation. The full $\mathcal{O}(\alpha)$ Z-exchange correction has been done with the BABAMC generator [8]. The electroweak correction is four times smaller for SiCAL with respect to LCAL due to the former's acceptance at lower angles. This reflects in a smaller theoretical uncertainty for the SiCAL Bhabha cross section [9]: the theoretical systematic error for LCAL is estimated to be 0.28% (as is 1991 [1]) and 0.25% for SiCAL. The separate contributions are summarized in Table 2.

3   Measurements of Cross Sections and Forward-Backward Asymmetries

The selections for hadronic and leptonic events, except the $\tau^+\tau^-$ selection, are not changed from those in [1, 2]. The evaluations of the selection systematics for the hadrons, Bhabhas and muon-pairs are

Contribution	LCAL	SiCAL
(1) $\mathcal{O}(\alpha^2)$ LL BHLUMI	0.15%	0.15%
(2) $\mathcal{O}(\alpha^2)$ SL BHLUMI	0.09%	0.09%
(3) Z-exchange $\mathcal{O}(\alpha)$ BABAMC	0.03%	0.03%
(4) Z-exchange $\mathcal{O}(\alpha^2)$ LL missing in BABAMC	0.06%	0.015%
(5) Z-exchange $\mathcal{O}(\alpha^2)$ SL missing in BABAMC	0.06%	0.015%
(6) Vacuum polarization	0.08%	0.05%
Total theoretical uncertainty	0.28%	0.25%

Table 2: Summary of theoretical systematic errors from [9] for the two luminosity reference cross sections. QED leading-log (LL) and sub-leading (SL) uncertainties (1 and 2) and the Z-exchange correction uncertainties (4 and 5) are each added linearly.

discussed below. The improved $\tau^+\tau^-$ selection and its corresponding systematic error are presented in detail. The flavor-blind lepton selection, called "common lepton" hereafter, has not been changed from [1, 2].

The measured cross sections for the hadronic (selections averaged) and lepton-pair final states are shown in Table 3. The lepton forward-backward asymmetries A_{FB}, presented in Table 4 are determined by a maximum likelihood fit of the function

$$\frac{d\sigma}{d\cos\theta^*} = C \cdot (1 + \cos^2\theta^* + \frac{8}{3}A_{FB}\cos\theta^*) \cdot F(\cos\theta^*) \tag{1}$$

to the $\cos\theta^*$ angular distributions. The scattering angle, θ^*, is defined as

$$\cos\theta^* = \cos\frac{1}{2}(\theta_1 + \pi - \theta_2)/\cos\frac{1}{2}(\theta_1 - \pi + \theta_2), \tag{2}$$

where θ_1 and θ_2 are the polar angles of the vector sum of the track momenta in the hemispheres corresponding to the outgoing lepton and antilepton [2]. $F(\cos\theta^*)$ describes the effect of the t-channel exchange for the $e^+ e^-$ channel and C is a normalization constant.

3.1 Hadronic Selection Systematics

Two hadron selection methods are used, one based on the energy and multiplicity of charged particles in the Time Projection Chamber (TPC) and the other based on the total calorimetric energy. The efficiencies are 97.47% and 99.07% respectively, where the loss in efficiency for the charged-track selection comes essentially from low-angle events which fail either the multiplicity or the energy cuts. The cross sections are given in Table 3 for the individual selections and for their average. The event selection cuts out events with large initial state radiation. The cross sections are given corrected up to $\sqrt{s'} > 0.1\sqrt{s}$, where $\sqrt{s'}$ is the mass of the e^+e^- pair after initial state radiation.

Increased data and higher Monte Carlo statistics have improved the understanding of the tau pair

Measurement		LCAL period	SiCAL period
$\mathcal{L}_{int}$ (nb^{-1})		13684.0 ± 23.4 ± 43.8 ± 38.3 (th.)	8749.0 ± 10.2 ± 13.1 ± 21.9 (th.)
Number of selected $q\bar{q}$		415803	264610
ee		16647	10725
$\mu\mu$		17082	10879
$\tau\tau$		16274	10385
common leptons		58566	37607
σ_{had} (nb)	Charged tracks:	30.719 ± 0.071 ± 0.141	30.575 ± 0.070 ± 0.103
σ_{had} (nb)	Calorimeter:	30.710 ± 0.071 ± 0.139	30.566 ± 0.069 ± 0.102
σ_{had} (nb)	Average:	30.715 ± 0.071 ± 0.137	30.570 ± 0.069 ± 0.099
σ_{ee} (nb)		1.506 ± 0.014 ± 0.009	1.519 ± 0.017 ± 0.007
$\sigma_{\mu\mu}$ (nb)		1.499 ± 0.012 ± 0.009	1.484 ± 0.014 ± 0.008
$\sigma_{\tau\tau}$ (nb)		1.497 ± 0.012 ± 0.008	1.494 ± 0.015 ± 0.007
$\sigma_{common\ leptons}$ (nb)		4.503 ± 0.024 ± 0.026	4.525 ± 0.027 ± 0.022

Table 3: Integrated luminosities, event numbers and hadron and lepton cross sections with statistical and systematic errors for 1992. The data are separated for running before SiCAL installation, LCAL period (91.276 GeV), and afterwards, SiCAL period (91.270 GeV). The theoretical error (th.) is shown explicitly for the luminosities. The luminosity errors (theoretical error included) are added in quadrature in the cross sections shown here.

background in the calorimetric selection. The correction is $(0.46 \pm 0.06)\%$, where the uncertainty is reduced by more than a factor two with respect to the previous publications [1, 2].

The systematic error of the charged track based selection has been re-evaluated to take advantage of the increased statistics. The backgrounds are small, $(0.32 \pm 0.03)\%$ coming from $\tau^+\tau^-$ events and $(0.25 \pm 0.08)\%$ from two-photon interactions. The limited precision in the simulation of the detector response for the cut variables [2] is responsible for a systematic error of $0.4 \cdot 10^{-3}$.

The uncertainty in the extrapolation to full acceptance coming from the hadronization model has been estimated using real events in which the thrust axis is nearly normal to the beam direction ($|\cos\theta_{Thrust}| < 0.2$). The events were rotated randomly in space and tracks falling outside the detector acceptance were eliminated. The acceptance was then recalculated by weighting the events passing the hadron selection with the proper thrust angular distribution. This procedure was repeated with fully simulated events. A difference in the efficiency of $(1.1 \pm 0.4) \cdot 10^{-3}$ was found. The selected events are well contained in the detector, the loss in average track multiplicity being < 1%; the probability that they are not identified as hadronic events is negligible. However, two classes of hadronic decays are not represented in the sample: low charged multiplicity events and events with strong initial state bremsstrahlung. Although the second class is well simulated in the Monte Carlo, the uncertainty in the fraction of events of the first class is large. The estimated uncertainty due to these events is $0.8 \cdot 10^{-3}$, giving a total uncertainty in the efficiency of $1.4 \cdot 10^{-3}$. Combining all the errors assigned to detector response, Monte Carlo, background

12

Measurement	LCAL + SiCAL periods
A_{FB}^{ee}	$0.0115 \pm 0.0074 \pm 0.0029$
$A_{FB}^{\mu\mu}$	$0.0101 \pm 0.0059 \pm 0.0010$
$A_{FB}^{\tau\tau}$	$0.0052 \pm 0.0067 \pm 0.0005$

Table 4: Forward-backward asymmetries for lepton pairs. The data are presented for the combined LCAL and SiCAL periods, where the average energy is 91.274 GeV. Both the statistical and systematic errors are given.

and modeling gives a total systematic error for the track-based selection of $1.7 \cdot 10^{-3}$.

The systematic errors for both selections are summarized in Table 5. Since they use different detector components for the identification, the two selections are considered independent. Therefore the systematic error of the average is obtained by combining the systematic errors of the two selection efficiencies, assuming they are uncorrelated, with the other uncertainties (Monte Carlo statistics and background), assuming they are fully correlated between both selections. The overall systematic uncertainty in the combined cross section is then 0.14%.

	Hadronic selection	
Source	Charged track	Calorimeter
detector response	0.4	1.1
modeling	1.4	negl.
Monte Carlo stat.	0.4	0.4
background:		
$\gamma\gamma$	0.8	0.8
e^+e^-	negl.	0.3
$\tau^+\tau^-$	0.3	0.6
Total	1.7	1.6

Table 5: Systematic errors (10^{-3}) for hadronic selections.

3.2 $Z \to e^+ e^-$ Selection Systematics

The selection of electron pairs is based on the sum of the momenta of the two tracks with highest momenta and the sum of the energy in the electromagnetic calorimeter and in the regions of the hadron calorimeter along the cracks of the electromagnetic one. The selection efficiency and the τ background

systematic errors have been re-evaluated since [1]; the error on the global efficiency and τ background together is 0.3%. The uncertainty in the extreme backward bin of $\cos\theta^*$, $[-0.9, -0.8]$, was re-evaluated by moving the most sensitive cut, the one on the sum of momenta and calorimetric energy [2], by $\pm 10\%$. Agreement between data and Monte Carlo is consistent with a 1% uncertainty for this bin. The resulting total systematic error for the cross section is 0.41%, and the error for the A_{FB} measurement is 0.29%. The theoretical uncertainty in the t-channel subtraction due to inherent limitations of the calculation in the ALIBABA program [10] contributes 0.23% and 0.25% to these errors, respectively.

The number of selected events (before corrections, t-channel subtraction, etc.), measured cross section and forward-backward asymmetry are given in Tables 3 and 4.

3.3 $Z \rightarrow \mu^+\mu^-$ Selection Systematics

The selection of muon-pair events is based on their penetrating power, which leads to signals in the last planes of the hadron calorimeter and in the two layers of muon chambers that surround ALEPH [2]. The systematic error for the μ-pair cross section is unchanged from [1], 0.5%. Two studies have been used to set an upper limit on the systematic error for the measurement of the forward-backward asymmetry. First, a comparison has been made between the standard selection and the one based on minimum ionizing signals in ECAL and HCAL [2], both of which have different background components. An uncertainty of $7 \cdot 10^{-4}$ on A_{FB} is inferred from the difference between both selections. Second, the accuracy of the tracking in the very forward region has been studied by enlarging the selection to accept tracks with $|\cos\theta| < 0.98$ and events with $|\cos\theta^*| < 0.95$. An upper limit of $6 \cdot 10^{-4}$ is obtained for the systematic error from this source. Adding the uncertainties from both sources in quadrature gives a total systematic uncertainty on A_{FB} of 0.10%.

The number of selected events, and values of the measured cross section and forward-backward asymmetry are shown in Tables 3 and 4.

3.4 Improved $Z \rightarrow \tau^+\tau^-$ Selection and Systematics

3.4.1 $\tau^+\tau^-$ Selection and Cross Section

The new selection of τ-pair events starts by dividing the event in two hemispheres by a plane perpendicular to the thrust axis. Two "jets" are defined by clustering together all charged and neutral objects present in each hemisphere, which are found using the energy flow algorithm described in [11]. The τ direction is given by the vectorial sum of the momenta of all the objects in the jet. The most energetic charged track in each hemisphere is called leading track.

The event is required to have at least 2 and at most 8 charged tracks in the polar angular range $|\cos\theta| < 0.95$ and at least one charged track in each hemisphere. The scattering angle θ^*, defined using the charge and the direction of jets, has to satisfy the condition $|\cos\theta^*| < 0.9$. In order to reduce the $\gamma\gamma$ background the event must have an acollinearity, defined as $180°$ minus the angle between the two jets, smaller than $20°$, and either a ratio of total reconstructed energy, E_{rec}, to beam energy, E_{beam}, $E_{rec}/E_{beam} > 0.350$ or an absolute difference between the transverse momenta of the jets greater than 3 GeV/c. Cosmic ray reduction is obtained by asking for at least one charged track to originate from within a cylinder of length 10 cm and radius 2 cm coaxial with the beam and centered on the measured collision point. If both hemispheres have either more than one charged track or an invariant mass greater than 1 GeV/c^2, further cuts are applied to reject hadronic events. Defining $n_{ob,i}$ and θ_i^{op} as the number of charged and neutral objects and the maximum angle between two charged tracks in the hemisphere i respectively, the requirements are $n_{ob,1} \cdot n_{ob,2} < 75$ and $\theta_1^{op} + \theta_2^{op} < 0.25$ rad.

14

Bhabha and dimuon events are rejected by requiring the sum of the energy of the two leading charged tracks to be less than $1.6 \cdot E_{beam}$. The fractions of Bhabha and dimuon events remaining at this level are 17% and 2.5% respectively. The remaining events are then tagged using the lepton identification described in [11] applied with very loose cuts to keep a high efficiency. In addition, charged tracks less than 3 cm away from ECAL cracks are called *electrons* if they are not identified as muons. *Bhabha-like* events, i.e. events where all the charged tracks are identified as electrons, are rejected using two variables. First, the total energy is found as $E_{tot} = E_{rec} + E_{rad}$, where E_{rad} is the energy of a radiated photon collinear to the beam, computed using the jet directions and imposing 4-momentum conservation. Second, in order to tag possible losses of photons due to ECAL cracks, a variable ($D_{g,i}$) is defined by taking the tangent to the leading track in each hemisphere at the origin, extrapolating it to ECAL, and computing its minimum distance from a crack. Bhabha rejection is then obtained by applying a staggered cut in the variables $D_{min} = min(D_{g,1}, D_{g,2})$ and E_{tot}. The τ-pair events must have $E_{tot}/E_{beam} < 1.6$ when $D_{min} > 6$ cm, or $E_{tot}/E_{beam} < 1.4$ when $D_{min} < 6$ cm (see fig. 3a and b). *Dimuon-like* events are defined either if both leading tracks are identified as muons, or if one leading track is identified as a muon and the opposite hemisphere has a momentum in excess of $0.9 \cdot E_{beam}$. Dimuon rejection is obtained by requiring $E_{tot}/E_{beam} < 1.8$. Figure 3c) shows the E_{tot} distribution for data and simulated dimuon events.

After this selection 26 659 events remain. The overall acceptance is $78.12 \pm 0.23\%$, arising from an angular acceptance of 85.7% and a selection efficiency inside the acceptance of $91.16 \pm 0.27\%$. The error has been obtained by combining the uncertainties from the selection criteria, evaluated either by comparing data with Monte Carlo or by using artificial tau pairs formed from the data with tau's from different events [2]. The most important uncertainty comes from hadron rejection cuts due to the limited statistics of such artificial tau pairs. Backgrounds from electron pairs, muon pairs, and cosmic rays have been estimated using data to be respectively $(0.66 \pm 0.14)\%$, $(0.25 \pm 0.05)\%$, and $(0.17 \pm 0.03)\%$. Monte Carlo simulations of $\gamma\gamma$ and hadronic events have been used to estimate the contamination to be $(0.31 \pm 0.04)\%$ and $(0.25 \pm 0.03)\%$ respectively. The overall background subtraction amounts to $(1.64 \pm 0.16)\%$. The number of selected events and the cross section are given in Table 3 for LCAL and SiCAL periods. The systematic error is the sum in quadrature of background, efficiency and luminosity contributions.

3.4.2 $\tau^+\tau^-$ Forward-Backward Asymmetry

The measurement of the forward-backward asymmetry, $A_{FB}^{\tau\tau}$, requires additional cuts in order to minimize the bias from the remaining Bhabha background. To account for possible effects from a non-uniform efficiency with $\cos\theta^*$, A_{FB} has been measured differentially in five bins of $\cos\theta^*$, the final result being the weighted mean of the five values. Events are required to have one or three charged tracks per hemisphere and zero total charge. In the one prong–one prong (1-1) subsample Bhabha events are reduced to a negligible level either, 1) if one track is identified as an electron, by asking $E_{tot}/E_{beam} < 1.7$ when $|\cos\theta^*| < 0.72$, and < 1.4 otherwise, or 2) if both tracks are identified as electrons, by requiring the energy ratio to be smaller than 1.2 and 0.6, respectively.

After these additional requirements the number of selected events is 22 063. The Bhabha contamination is determined from the data to be smaller than $2.5 \cdot 10^{-3}$, giving rise to a $4.5 \cdot 10^{-4}$ systematic error on A_{FB}. The residual symmetrical contamination amounts to $(0.40 \pm 0.04)\%$, giving a contribution to the uncertainty in A_{FB}, of $\pm 0.6 \cdot 10^{-4}$. The probability to mis-measure the electric charge in a hemisphere, measured by studying the total charge distribution for 1-1 and 1-3 events, is found to be smaller than 10^{-2}, giving a correction to A_{FB} below 10^{-4}. The effect of track-insensitive regions in the Time Projection Chamber is negligible because of the $|\cos\theta^*|$ cut at 0.9. The same effect in the calorimeters is investigated by comparing hemispheres which are selected only based on charged tracks with hemispheres which include calorimeter energy. The estimate of the systematic error due to this effect is $2.5 \cdot 10^{-4}$. The $A_{FB}^{\tau\tau}$ value for the combined LCAL and SiCAL periods is given in Table 4.
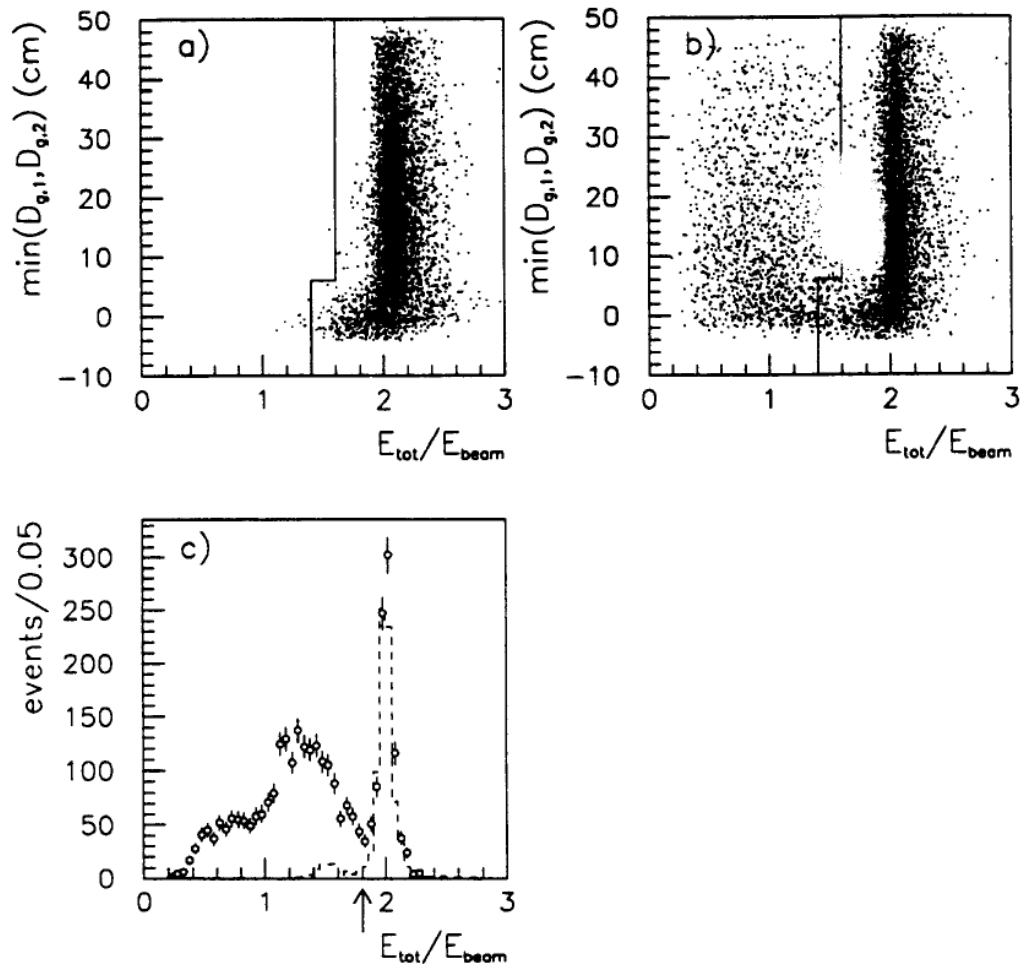
15

Figure 3: a) Minimum distance of the leading tracks to an ECAL crack versus E_{tot} for Bhabha Monte Carlo events; b) the same distribution for Bhabha-like events in the data; c) E_{tot} distribution for data satisfying dimuon-like criteria (open circles) and dimuon Monte Carlo events (dashed histogram). See text for definitions.

16

The determination of A_{FB} was repeated using the selection previously published [1, 2], based mainly on identifying muons and pions using information from the calorimeters. In addition the Bhabha background has been reduced by 75% with respect to [1] with a combined cut on track momentum and energy in the electromagnetic calorimeter, $E_{cal}^2 + P^2$. The selection efficiency is 84% within $|\cos\theta| < 0.9$. The result is $A_{FB}^{\tau\tau} = 0.0048 \pm 0.0065$. The systematic error of this analysis was evaluated and found to be 0.0005, essentially from the same sources as in the analysis above, and also applies to the previously published $A_{FB}^{\tau\tau}$ data [1, 2]. The forward-backward asymmetries from the two selection procedures agree and have negligible systematic errors. Since the new selection is also used for the determination of the tau-pair cross section, its value for the forward-backward asymmetry is given in Table 4.

3.5 Common Lepton Cross Section

The flavour-blind lepton-pair selection is based on the measurement of charged particles and does not attempt to identify the individual lepton species. The selection has not been changed from [1, 2]. The resulting cross section is given in Table 3. Its systematic error remains the same, 0.4%, and is essentially independent to the systematic errors of the individual lepton analyses, which come mainly from particle identification. As a cross-check of the systematic errors of the individual lepton analyses, the cross-section obtained with the common lepton selection has been compared with the sum for the three individual lepton channels. The difference for the two periods combined is

$$\sigma_{\text{common leptons}} - (\sigma_{ee} + \sigma_{\mu\mu} + \sigma_{\tau\tau}) = (0.012 \pm 0.007)\,\text{nb} \tag{3}$$

where the error includes only the non-common statistical uncertainty.

4 Fits to Cross Sections and Forward-Backward Asymmetries

The 1992 hadron and individual lepton cross sections and forward-backward asymmetries were fit along with the accumulated 1989, 1990 and 1991 ALEPH data using the MIZA [12] lineshape fitting program as in [1] updated with the results in [13]. A 5-parameter fit assuming lepton universality and a 9-parameter fit without lepton universality are made in the same way as in [1]. The results are shown in Table 6. In the following R_l is defined as the ratio of the Z hadronic partial width to the leptonic partial width, Γ_{ll}, for massless final-state leptons (obtained from R_e, R_μ and R_τ correcting for mass effects). The 1992 data taken at the Z peak do not contribute to the values of M_Z and Γ_Z, both of which remain unchanged from [1]. The errors in the peak forward-backward asymmetries, $A_{FB}^{0,l}$, include a 0.0010 component from the uncertainty in the LEP center of mass energies.

The fit parameters can be used to derive the leptonic and hadronic partial widths, Γ_{ll} and Γ_{had}, respectively, their branching ratios and the invisible width, $\Gamma_{inv} = \Gamma_Z - \Gamma_{had} - (\Gamma_{ee} + \Gamma_{\mu\mu} + \Gamma_{\tau\tau})$. The results are shown in Table 7. Using the electroweak Standard Model value for Γ_ν/Γ_{ll} (1.992 ± 0.003), the ratio of the invisible width to the leptonic one, assuming $\Gamma_{inv} = N_\nu\Gamma_\nu$, gives the number of light neutrino species

$$N_\nu = 2.983 \pm 0.034.$$

Alternatively, assuming three neutrino species allows one to determine the ratio $\Gamma_\nu/\Gamma_{ll} = 1.981 \pm 0.022$.

Both σ_h^0 and R_l, within the context of the minimal Standard Model, depend weakly on the masses of the top quark and Higgs boson, making them ideal parameters to test for departures from the standard electroweak theory. The principal remaining uncertainty comes from the dependence of R_l and to a more

Parameter	No lepton univ.	Lepton univ.
M_Z (GeV)	91.187 ± 0.009	91.187 ± 0.009
Γ_Z (GeV)	2.501 ± 0.012	2.501 ± 0.012
σ_h^0 (nb)	41.60 ± 0.16	41.60 ± 0.16
R_e	20.59 ± 0.15	—
R_μ	20.83 ± 0.15	—
R_τ	20.70 ± 0.16	—
R_l	—	20.69 ± 0.09
$A_{FB}^{0,e}$	0.0185 ± 0.0066	—
$A_{FB}^{0,\mu}$	0.0146 ± 0.0048	—
$A_{FB}^{0,\tau}$	0.0197 ± 0.0056	—
$A_{FB}^{0,l}$	—	0.0171 ± 0.33
χ^2	147/150 d.o.f.	149/154 d.o.f.

Table 6: Fit results for cross sections and forward-backward asymmetries using all the ALEPH accumulated data (1989, 1990, 1991 [1] and 1992). The full correlation matrices for the results are given in Appendix A.

limited degree σ_h^0 on the strong coupling constant α_s. Figure 4 shows the probability contours for the parameters R_l and σ_h^0 given by the fit, along with the Standard Model prediction for 3 light neutrino generations, using a third-order expansion in α_s in the $\overline{MS}$ scheme as in [1]. The value of α_s shown in Table 7 is obtained from R_l using the formula

$$R_l = R_l^0 \left(1 + 1.05 \frac{\alpha_s}{\pi} + (0.9 \pm 0.1) \left(\frac{\alpha_s}{\pi} \right)^2 - 13 \left(\frac{\alpha_s}{\pi} \right)^3 \right), \tag{4}$$

where $R_l^0 = 19.936 \pm 0.029$ in the Standard Model[2]. The central value assumes top quark and Higgs masses of 150 GeV and 300 GeV respectively, and the error includes the effects of changing the top mass from 100 GeV to 200 GeV and the Higgs mass from 60 GeV to 1 TeV.

The vector and axial vector couplings to fermions are determined from the forward-backward asymmetries and the leptonic partial widths. $A_{FB}^{0,l}$ is used to obtain the ratio of the vector and axial vector couplings

$$g_V^2(M_Z^2)/g_A^2(M_Z^2) = 0.0058 \pm 0.0011$$

assuming lepton universality. This is interpreted as a measurement of the weak effective mixing angle, $\sin^2 \theta_{eff}^{lept} \equiv \frac{1}{4} (1 - g_V(M_Z^2)/g_A(M_Z^2))$, according to the definition used in [18]:

$$\sin^2 \theta_{eff}^{lept} = 0.2310 \pm 0.0019$$

The 9-parameter fit is repeated using the additional constraint coming from the measurement of τ polarization [14] from the 1989-1991 ALEPH data sample, to give improved results for the effective vector couplings shown in Table 8. Using these results together with the previous ALEPH measurements of the

---

[2]The calculation has been done using the electroweak library of the MIZA program
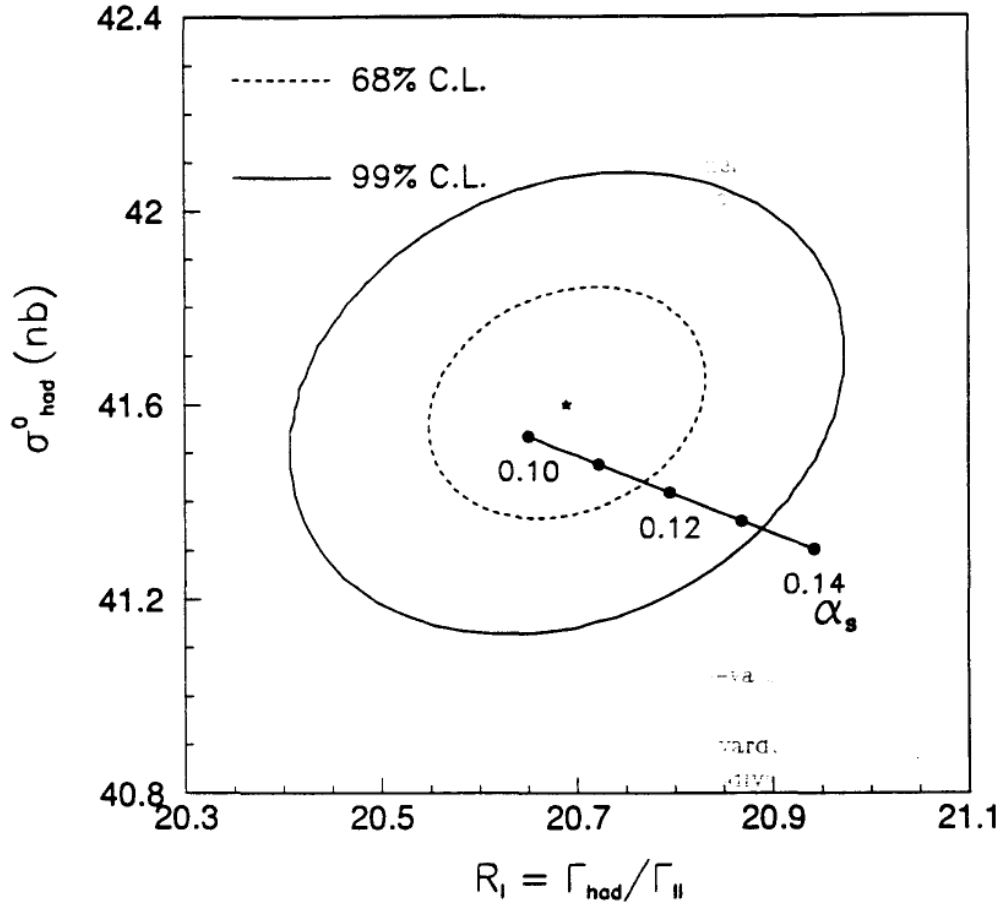
Figure 4: Contours of constant χ^2 for σ_h^0, the hadronic peak cross section, as a function of $R_l = \Gamma_{had}/\Gamma_{ll}$ together with the Standard Model prediction as a function of the QCD coupling constant $\alpha_s(M_Z^2)$.

Derived parameter	No lepton univ.	Lepton univ.
Γ_{had} (MeV)	—	1746 ± 10
Γ_{ll} (MeV)	—	84.40± 0.43
Γ_{inv} (MeV)	—	501 ± 6
Γ_{inv}/Γ_{ll}	—	5.942 ± 0.067
Γ_{ee} (MeV)	84.61 ± 0.49	—
$\Gamma_{\mu\mu}$ (MeV)	83.62 ± 0.75	—
$\Gamma_{\tau\tau}$ (MeV)	84.18 ± 0.79	—
Br(Z → hadrons) (%)	69.66 ± 0.29	69.83 ± 0.23
Br(Z → l^+l^-) (%)	—	3.375 ± 0.009
Br(Z → e^+e^-) (%)	3.383 ± 13	—
Br(Z → $\mu^+\mu^-$) (%)	3.344 ± .26	—
Br(Z → $\tau^+\tau^-$) (%)	3.366 ± 0.028	—
σ^0_{ll} (nb)	—	2.011 ± 0.010
σ^0_{ee} (nb)	2.021 ± 0.015	—
$\sigma^0_{\mu\mu}$ (nb)	1.997 ± 0.015	—
$\sigma^0_{\tau\tau}$ (nb)	2.010 ± 0.016	—
α_s	—	0.108 ± 0.012
$g_{Vl}(M_Z^2)$	—	-0.038 ± 0.004
$g_{Al}(M_Z^2)$	—	-0.502 ± 0.001
$g_{Ve}(M_Z^2)$	$-0.040^{+0.008}_{-0.007}$	—
$g_{Ae}(M_Z^2)$	-0.503 ± 0.002	—
$g_{V\mu}(M_Z^2)$	$-0.031^{+0.011}_{-0.013}$	—
$g_{A\mu}(M_Z^2)$	-0.501 ± 0.002	—
$g_{V\tau}(M_Z^2)$	$-0.042^{+0.013}_{-0.016}$	—
$g_{A\tau}(M_Z^2)$	-0.502 ± 0.003	—

Table 7: Derived quantities from fit results for all the ALEPH accumulated data (1989, 1990, 1991 [1] and 1992).

quark charge asymmetry (1989-1990) [15] and b and c forward-backward asymmetries (1990-1991) [16], the weak mixing angle becomes

$$\sin^2 \theta^{lept}_{eff} = 0.2321 \pm 0.0012 \quad (\chi^2/d.o.f. = 3.3/5).$$

5 Mass of the Top Quark

The lineshape information and the effective weak mixing angle presented in the previous section can be used, within the context of the minimal Standard Model, to determine the top quark mass and the strong coupling constant, as presented in [1]. In this analysis M_H is fixed at 300 GeV, and varied from 60 GeV to 1000 GeV to assess its effect on the uncertainty on the two parameters.

Fitting to the results for M_Z, Γ_Z, R_l, σ^0_h, $\sin^2 \theta^{lept}_{eff}$ and the previously published measurement of

Derived parameter	No lepton univ.
$g_{V_e}(M_Z^2)$	-0.036 ± 0.005
$g_{V_\mu}(M_Z^2)$	-0.034 ± 0.013
$g_{V_\tau}(M_Z^2)$	-0.038 ± 0.005

Table 8: Effective vector coupling constants from fit results for all the ALEPH accumulated data (1989, 1990, 1991 [1] and 1992) using the added constraint of τ polarization.

$\Gamma_{b\bar{b}}$ [17] yields the top quark mass and the strong coupling constant:

$$m_t = (184^{+25+17}_{-29-18})\,\text{GeV} \quad \text{and}$$
$$\alpha_s = 0.113 \pm 0.011 \pm 0.002,$$

with $\chi^2/d.o.f. = 6.1/8$, where the second error in each reflects the uncertainty due to the Higgs mass. The theoretical uncertainties have been treated as in [18]. In particular, the uncertainty in the low-energy hadronic part of the vacuum polarizations has been propagated in the fit and is included in the experimental error, which gets increased by about one GeV due to this. The probability contour is shown in fig. 5. The ALEPH results can be combined with information on M_W coming from neutrino experiments [19] and $\bar{p}p$ colliders [20]. In this case the result is

$$m_t = (172^{+20+17}_{-22-18})\,\text{GeV} \quad \text{and}$$
$$\alpha_s = 0.114 \pm 0.011 \pm 0.002,$$

with $\chi^2/d.o.f. = 7.3/11$. All results in sections 4 and 5 are in good agreement with the values published previously [1, 22].

6 Limits on Extra Z Bosons

As an example of the importance of the improved measurement of σ_h^0 in tests for departures from the Standard Model, a search for extra Z bosons of one particular E_6-based model (the χ-model [24]) is presented here.

After specifying the particular model (and without any assumption on the structure of the Higgs sector), there are only two free parameters

- The mixing angle between the symmetry eigenstates, Z^0 and $Z^{0\prime}$, which will be called θ_3.

- The mass of the heavier mass-eigenstate, that will be represented by $M_{Z'}$.

Data taken at LEP are mainly sensitive to θ_3 and only weakly to $M_{Z'}$, therefore only the θ_3 determination is presented. The sensitivity to the mixing angle comes from the fact that the mixing between the two neutral bosons leads to changes in the effective fermion couplings to the lower mass boson, which are different for charged and neutral leptons and for up- and down-type quarks [24]. The uncertainty related to the lack of knowledge of $M_{Z'}$ is included as part of the error in θ_3.
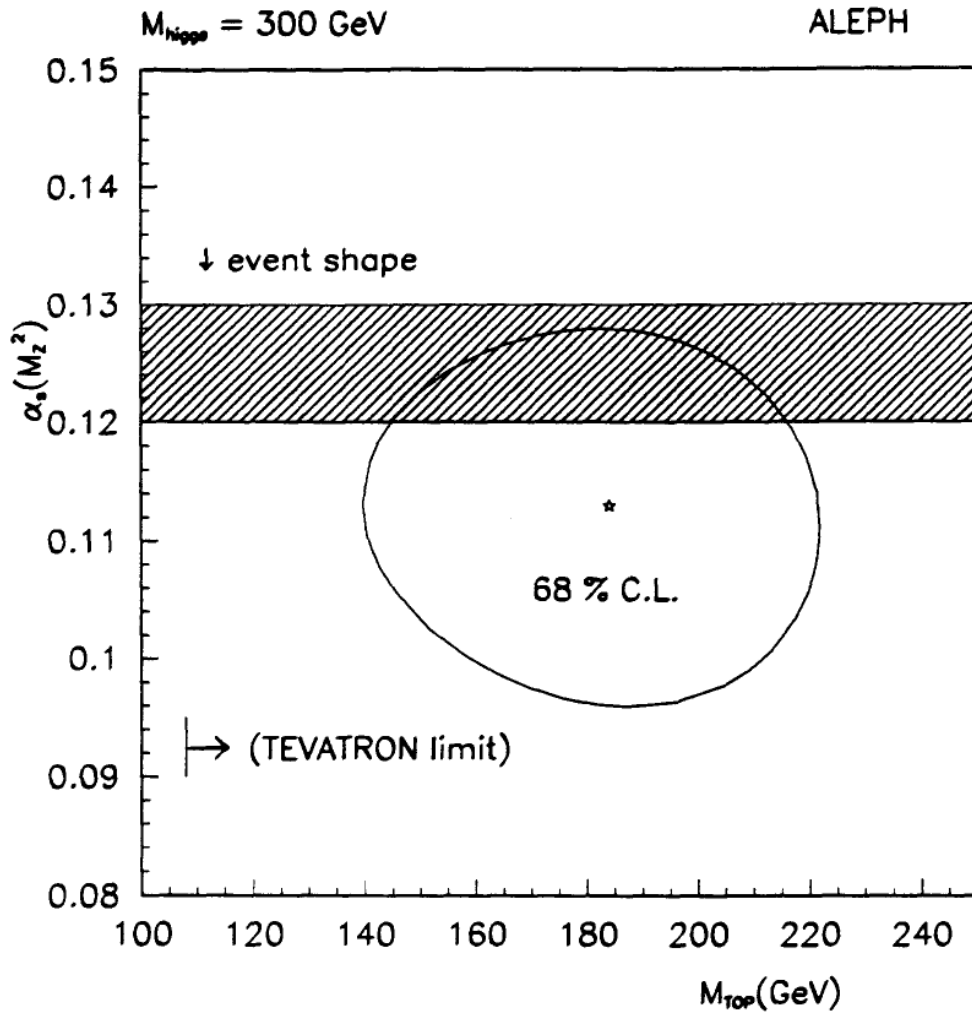
Figure 5: Contours of constant probability for the fit to the top quark mass, m_t, and the strong coupling constant, α_s. The results of the event shape analysis [21] for α_s are shown by the hashed band. The Tevatron limit refers to the result of [23].

First, the entire lineshape and asymmetry data, parametrized in terms of M_Z, Γ_Z, R_l, σ_h^0 and A_{FB}^0 are used together with a constraint on α_s from jet studies ($\alpha_s(M_Z^2) = 0.125 \pm 0.005$ [21]) to fit simultaneously for M_Z, m_t, α_s and θ_3 using the program of [25]. The result is

$$\theta_3 = (-3.4 \pm 2.9) \cdot 10^{-3}$$

for Higgs and Z' masses fixed at 300 and 500 GeV, respectively. Allowing the Higgs mass to vary from 60 to 1000 GeV and the Z' mass from 320 [26] to 1000 GeV, does not increase significantly the error on θ_3. No deviation is seen from the minimal Standard Model prediction ($\theta_3 = 0$), and a 95% confidence level limit on the value of the mixing angle can be set to

$$-0.0091 < \theta_3 < 0.0023 \,,$$

which is significantly more stringent than those published using results prior to 1992 [27, 28]. A similar conclusion is reached in [29] using preliminary 1992 results.

Second, in order to investigate the source of the sensitivity, a fit is made to get M_Z, α_s and θ_3 using only the experimental values of M_Z and σ_h^0 and the constraint on α_s, while fixing the top quark mass to 150 GeV. The resulting uncertainty on θ_3 is $\pm 3.3 \cdot 10^{-3}$, which increases to $\pm 3.4 \cdot 10^{-3}$ when the top quark mass is allowed to move between 100 and 200 GeV. The variation in Higgs and Z' masses mentioned above is included. Removing the hadronic peak cross section from the first fit, leaving the rest unchanged, increases the error to $\pm 5.8 \cdot 10^{-3}$, which implies that most of the sensitivity (with α_s constrained) comes from the measurement of σ_h^0. On the other hand, the constraint on α_s is also crucial in determining the mixing angle; removing it from the first fit increases the error on θ_3 by almost a factor two.

The qualitative picture deduced from these results does not change if different E_6 related models are chosen. The hadronic peak cross section, in conjunction with an external constraint on the strong coupling constant, is a powerful variable when testing for signals of extra neutral bosons.

7 Conclusion

In addition to a substantial increase in the data at the peak of the Z resonance, the increased precision in the luminosity measurement due to the new silicon-tungsten luminosity monitor, as well as improvements in the understanding of the hadron selection accuracy and the tau-pair selection algorithm, have substantially reduced previous uncertainties in the parameters of the Z resonance, especially the hadronic peak cross section. All results are consistent with the Standard Model. In this frame, the number of neutrino families is found to be $N_\nu = 2.983 \pm 0.034$, the effective weak mixing angle determined from the lepton-pair forward-backward asymmetries is $\sin^2 \theta_{eff}^{lept} = 0.2310 \pm 0.0019$. Including the previous ALEPH measurements of the tau polarization and polarization asymmetry, the quark charge asymmetry, and b and c forward-backward asymmetries gives $\sin^2 \theta_{eff}^{lept} = 0.2321 \pm 0.0012$. The top quark mass in this frame, including the results from $\Gamma_{b\bar{b}}$, is $m_t = (184_{-29-18}^{+25+17})$ GeV and $\alpha_s = 0.113 \pm 0.011 \pm 0.002$.

8 Acknowledgements

to the successful performance of ALEPH. Those of us from non-member countries thank CERN for its hospitality.

References

[1] D. Buskulic et al., ALEPH Collab., Z. Phys. C60 (1993) 71.

[2] D. Decamp et al., ALEPH Collab., Z. Phys. C53 (1992) 1;
D. Decamp et al., ALEPH Collab., Z. Phys. C48 (1990) 365.

[3] D. Decamp et al., ALEPH Collab., Nuclear Instruments and Methods A294 (1990) 121.

[4] D. Bédérède et al., *SiCAL - A High Precision Silicon-Tungsten Luminosity Calorimeter for ALEPH*, paper in preparation for Nuclear Instruments and Methods.

[5] L. Arnaudon et al., *The Energy Calibration of LEP in 1992*, CERN-SL/93-21 (DI) 1993.

[6] D. Decamp et al., ALEPH Collab., Z. Phys. C53 (1992) 375.

[7] S. Jadach, E. Richter-Wąs, Z. Wąs and B.F.L. Ward, Phys. Lett. B268 (1991) 253;
S. Jadach, E. Richter-Wąs, Z. Wąs and B.F.L. Ward, Comput. Phys. Commun. 70 (1992) 305;
S. Jadach and B.F.L. Ward, Phys. Rev. D40 (1989) 3582.

[8] M. Böhm, A. Denner and W. Hollik. Nucl. Phys. B304 (1988) 687;
F.A. Berends, R. Kleiss and W. Hollik. Nucl. Phys. B304 (1988) 712.

[9] W. Beenakker and B. Pietrzyk, Phys. Lett. B304 (1993) 366; W. Beenakker and B. Pietrzyk, Phys. Lett. B296 (1992) 296.

[10] W. Beenakker, F. A. Berends and S. C. van der Marck, Nucl. Phys. B349 (1991) 323.

[11] D. Decamp et al., ALEPH Collab., Phys. Rep. 216 (1992) 253.

[12] M. Martinez, L. Garrido, R. Miquel, J.L. Harton and R. Tanaka, Z. Phys. C49 (1991) 645.

[13] B. A. Kniehl and A. Sirlin, Phys. Rev. D47 (1993) 883;
S. Fanchiotti, B. A. Kniehl and A. Sirlin, Phys. Rev. D48 (1993) 307;
R. Barbieri et al., Phys. Lett. B288 (1992) 95;
K. G. Chetyrkin, J. H. Kühn, Phys. Lett. B248 (1990) 359;
K. G. Chetyrkin, J. H. Kühn and A. Kwiatkowski, Phys. Lett. B282 (1992) 221;
J. Fleischer, O. V. Tarasov and F. Jegerlehner, Phys. Lett. B293 (1992) 437.

[14] D. Buskulic et al., ALEPH Coll., Z. Phys. C59 (1993) 369.

[15] D. Decamp et al., ALEPH Coll., Phys. Lett. B259 (1991) 377.

[16] D. Buskulic et al., ALEPH Coll., CERN-PPE/94-17.

[17] D. Buskulic et al., ALEPH Coll., Phys. Lett. B313 (1993) 535; Phys. Lett. B313 (1993) 549.

[18] The LEP collaborations, *Updated Parameters of the Z^0 Resonance from Combined Preliminary Data of the LEP Experiments*, CERN/PPE/93-157 (26 August 1993).

[19] C. G. Arroyo et al., CCFR Coll., Columbia University preprint NEVIS R#1498, November 1993.
H. Abramowicz et al., CDHS Coll., Phys. Rev. Lett. 57 (1986) 298; A. Blondel et al., Z. Phys. C45 (1990) 361.
J. V. Allaby et al., CHARM Coll., Phys. Lett. B177 (1986) 446; Z. Phys. C36 (1987) 611.

[20] J. Alitti et al., UA2 Coll., Phys. Lett. B241 (1990) 150.
F. Abe et al., CDF Coll., Phys. Rev. Lett. 65 (1990) 2243.

[21] D. Decamp at al., ALEPH Coll., Phys. Lett. B284 (1992) 163.

[22] P. Abreu et al., DELPHI Coll., CERN-PPE/94-08.
O. Adriani et al., L3 Coll., Phys. Rep. 236 (1993) 1.
R. Akers et al., OPAL Coll., CERN-PPE/93-146.

[23] A. Barbiero-Galtieri, plenary talk at the EPS Conference, Marseille, July 1993. Recently, the D0 collaboration has reported a more stringent limit on the top quark mass in S. Abachi et al., D0 Coll., FERMILAB-PUB-94-004-E.

[24] R. W. Robinett, Phys. Rev D26 (1982) 2388;
R. W. Robinett and J. L. Rosner, Phys. Rev D26 (1982) 2396;
F. del Aguila, G. Blair, M. Daniel, G. G. Ross, Nucl. Phys. B272 (1986) 413;
J .L. Hewett, T. G. Rizzo, J. A. Robinson, Phys. Rev. D33 (1986) 1476; ibid. D34 (1986) 2179;
D. London and J. L. Rosner, Phys. Rep. 34 (1986) 1530;
P. Binetruy, S. Dawson, T. Hinchliffe, M. Sher, Nucl. Phys. B273 (1986) 501;
J. Ellis, K. Enqvist, D. V. Nanopoulos, F. Zwirner, Nucl. Phys. B276 (1986) 14.
G. Belanger and S. Godfrey, Phys. Rev. D35 (1987) 378.

[25] A. Leike, S. Riemann and T. Riemann, University of Munich preprint LMU-91/06, and FORTRAN program ZEFIT;
A. Leike, S. Riemann and T. Riemann, Phys. Lett. B291 (1992) 187.

[26] F. Abe et al., CDF Collab., Phys. Rev. Lett. 68 (1992) 1463.

[27] O. Adriani et al., L3 Collab., Phys. Lett. B306 (1993) 187.

[28] P. Langacker and M. Luo, Phys. Rev. D45 (1992) 278;
E. Nardi, E. Roulet and D. Tommasini, Phys. Rev. D46 (1992) 3040;
F. del Aguila, W. Hollik, J. M. Moreno and M. Quiros, Nucl. Phys. B372 (1992) 1;
M. C. Gonzalez-Garcia and J. W. F. Valle, Phys. Lett. B259 (1991) 365;
G. Bhattacharyya et al., Mod. Phys. Lett. A6 (1991) 2552.

[29] G. Altarelli et al., Phys. Lett. B318 (1993) 139.

A Appendix

A.1 Correlation Matrix for 5-Parameter Fit

	Γ_Z	σ_h^0	R_l	$A_{FB}^{0,l}$
M_Z	0.017	0.022	-0.001	0.175
Γ_Z	—	-0.127	0.011	0.008
σ_h^0		—	0.216	0.009
R_l			—	0.007

A.2 Correlation Matrix for 9-Parameter Fit

	Γ_Z	σ_h^0	R_e	R_μ	R_τ	$A_{FB}^{0,e}$	$A_{FB}^{0,\mu}$	$A_{FB}^{0,\tau}$
M_Z	0.014	0.019	-0.002	0.002	-0.001	0.076	0.102	0.086
Γ_Z	—	-0.127	0.002	0.018	0.001	0.005	0.005	0.004
σ_h^0		—	0.137	0.133	0.130	0.005	0.006	0.005
R_e			—	0.078	0.072	0.005	0.000	0.000
R_μ				—	0.071	0.001	0.009	0.000
R_τ					—	0.000	0.000	0.007
$A_{FB}^{0,e}$						—	0.042	0.039
$A_{FB}^{0,\mu}$							—	0.040